# Scanning probe microscopy study of height-selected Ag/Ge(111) nanomesas driven by quantum size effects

F. Krok,[1,*] F. Buatier de Mongeot,[2] M. Goryl,[1] J. J. Kolodziej,[1] and M. Szymonski[1]
[1]*Research Center for Nanometer-Scale Science and Advanced Materials (NANOSAM), Faculty of Physics, Astronomy and Applied Computer Science, Jagiellonian University, ul. Reymonta 4, 30-059 Krakow, Poland*
[2]*Dipartimento di Fisica, Università di Genova, Via Dodecaneso 33, 16146 Genova, Italy*
(Received 30 November 2009; revised manuscript received 9 February 2010; published 10 June 2010)

We present scanning tunnel microscope, noncontact atomic force microscopy, Kelvin probe force microscopy, and low-energy electron diffraction study of the morphological evolution of Ag ultrathin films (0.5–6 ML) grown at 150 K on Ge(111)-$c(2\times8)$ substrate. Although the system has been widely studied in the context of quantum confinement effects in the electronic structure of these films, no real-space imaging has been reported so far. Our results demonstrate that upon annealing to room temperature, the Ag film adopts a (111) epitaxy on top of a wetting layer. It has been found that the Ag film adopts a metastable morphology which is determined by a delicate interplay between thermodynamics and the kinetics of interlayer mass transport. The preferential population of a discrete set of the deposit heights at 6, 10, and 12 ML suggests that quantum size effects are indeed active for the Ag/Ge system. Kelvin probe force microscopy indicates that the surface potential depends monotonically on the film thickness and does not show any oscillatory behavior in correspondence to the height changes.

DOI: 10.1103/PhysRevB.81.235414 PACS number(s): 73.21.Ac, 73.21.Fg, 68.37.Ps, 81.05.Cy

## I. INTRODUCTION

The quality of metallic overlayers grown on semiconductor substrates is crucial for their latter application. Atomically uniform epitaxial films are highly desired but in practice they are difficult to obtain. Depending on the deposition conditions, on the successive thermal annealing and on the amount of deposited material it was shown that, in the case of several metal/semiconductor systems, the resulting morphology can be switched from an atomically smooth to a columnarlike. One of the promising ways to produce smooth overlayers is to manipulate the kinetics of growth adopting a two-step approach.[1] First, deposition is performed at low temperatures, resulting in the formation of a compact and complete overlayer which, due to the reduced mobility of the deposited atoms, presents small scale roughness. Second, the substrate is annealed at temperatures for which diffusive transport becomes activated inducing a morphological equilibration and overall reduction in the film roughness down to the atomic scale, as seen for example, for Ag films grown on Fe(100) (Ref. 2) or on GaAs(110).[1]

The simple picture outlined above can, however, be deeply modified by a subtle interplay between kinetics and thermodynamics, leading to the formation of metastable columnar structures which imply the occurrence of massive interlayer mass transport. The best known example is probably that of Pb growth on Si(111) where, below a critical film thickness, the formation of multilayer islands with selected quantized heights is observed during the annealing process.[3] The driving force for such a fancy growth mode has been attributed to the occurrence of quantum size effects (QSE), in which the quantization of electronic energy states due to electron confinement in the direction perpendicular to the surface affects the energetic minima of the interface for specific film thicknesses.[4] The occurrence of QSE indicated by formation of islands with selected quantized heights has been also reported for the low-temperature (LT) grown and room-temperature (RT) annealed Ag/Si(111) system.[5,6]

For the closely related system Ag/Ge(111) the evidence of quantum size effects during growth have appeared so far more elusive although the electronic structure of this system presents strong similarities with that of Ag/Si(111). Indeed Ag/Ge(111) has been intensively investigated in detailed photoemission studies which have addressed the behavior of the quantum well states of the Ag film.[7–11] Also, according to the outcome of diffraction experiments, the growth of the Ag film has been reported to take place in a layer by layer fashion.[12]

In the present paper we report on scanning probe microscopy (SPM) studies of the growth of Ag films on Ge(111) substrate using the two-step procedure, LT deposition follow by a slow annealing to RT. The experiments, complemented by low-energy electron diffraction (LEED) measurements, demonstrate that the growth leads to formation of islands of quantized height during the thermal annealing step. These findings indicate that QSE affects the film morphology in a similar fashion to the case of Ag/Si(111).

The specific columnar morphology of the Ag/Ge(111) films selected by QSE and the spectroscopic evidence of the occurrence of vertical quantum confinement make the Ag/Ge(111) system a good candidate for testing the theory predicting the oscillatory dependence of the surface potential (work function) on the thickness of the overlayer due to change in the energy levels of the vertically confined metal electrons.[2,13] To address this issue we have performed spatially resolved surface potential measurements by means of Kelvin probe force microscopy (KPFM), an extension of the dynamic force microscopy (DFM) technique, which provides surface chemical sensitivity at the nanometer scale by means of surface contact potential difference (CPD) measurements.[14–17] The experiment provide clear evidence of a monotonic thickness-dependent CPD contrast with lat-

 

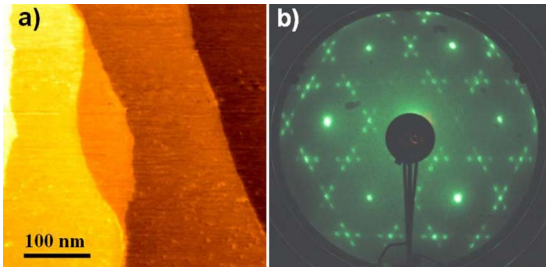


FIG. 1. (Color online) Nc-AFM topography image (a) of clean Ge(111) substrate surface with corresponding LEED pattern (b) exhibiting the $c(2\times8)$ surface reconstruction ($E=58$ eV).

eral resolution of few nm and energy resolution in the range of few meV.

## II. EXPERIMENTAL

The experiments were performed in UHV system consisting of three chambers for sample preparation, analysis, and SPM imaging, interconnected by magnetically coupled linear transfers. The base pressure in the system was of $5\times10^{-11}$ mbar. The Ge(111) samples were cut from commercial available wafers (Kelpin Crystal) and clamped with tungsten springs on a molybdenum plate supported on a copper sample holder. For improving thermal conductivity, a layer of gallium metal was placed between the crystal and the Mo plate. Prior to the introduction into the vacuum chamber, the Ge sample was cleaned with methanol, and while in vacuum, the sample was degassed overnight. Next, the sample was sputtered with 600 eV $Ar^+$ ion beams for 30 min at a sample temperature of about 900 K, as measured with a chromel-alumel thermocouple mounted on the side on the sample stage. Typically, a few cycles of sputter-cleaning were performed until a sharp $c(2\times8)$ LEED pattern of the Ge(111) clean surface was obtained.[18,19] This procedure routinely allows to achieve atomically flat terraces which exceed few hundred nanometers in width, as checked by SPM technique. Figure 1(a) shows an example of the clean Ge(111) surface obtained according the described procedure, while Fig. 1(b) presents the corresponding $c(2\times8)$ LEED pattern. The chemical cleanness of the obtained surface was checked with Auger electron spectroscopy (AES).

Ag was evaporated from a ceramic crucible at a rate of 0.3 ML/min which was calibrated with a quartz-crystal microbalance. Ag films of nominal thickness ranging from 0.5 to 6 ML were grown on Ge(111) at 150 K. During the growth the sample was cooled by a liquid nitrogen flow cryostat connected to the sample holder by a copper braid. To minimize the effects of substrate contamination due to the condensation of background gas, the sample stage was cooled prior to the transfer of the sample. The pressure in the chamber during the Ag film grown was in the low $10^{-10}$ mbar range. Immediately after Ag deposition at low temperature, the sample was transferred into the analysis chamber and gradually annealed to room temperature, while the process was monitored using LEED.

The morphology of the samples was assessed with an UHV scanning probe microscope. Both scanning tunneling microscopy (STM) and noncontact atomic force microscopy (nc-AFM) measurements were performed at room temperature after the completion of the annealing process which lasted at least 10 h. For the nc-AFM and KPFM measurements a modified VP2 AFM/STM Park Scientific Instruments device equipped with Nanosurf "easy-PLL" demodulator was used.[20] The topography was acquired using noncontact frequency modulated (FM) mode with a silicon (boron-doped) piezoresistive cantilever, purchased from Park Scientific Instruments, of resonance frequency of about 200 kHz. The frequency shift relative to the free cantilever resonance frequency was set in the range of −10 to −50 Hz at a constant oscillation amplitude of 10–20 nm. The tip prior to the measurements was cleaned in the UHV by thermal annealing to about 1100 K by passing a current through the resistive legs of the cantilever. For the CPD measurements with FM-KPFM,[16] the sample was biased with a dc voltage and ac voltage of frequency $f_{ac}=600$ Hz and amplitude $V_{ac}=300$ mV. The sample bias modulation was applied during the topography imaging so that the topography and CPD images were acquired simultaneously. The time variable electrostatic tip-sample interaction modulated at the frequency $f_{ac}$-induced synchronized variation in the frequency shift ($df$). The $f_{ac}$ component of the $df$ was detected through the lock-in amplifier (Stanford Research Systems, SR510) and an additional feedback loop (Kelvin controller) was used to provide the dc component of the sample bias in order to compensate the contact potential difference between the tip and the sample surface. As a result, the acquired dc map represents the distribution of the local surface electrostatic potential. The scanning rate for CPD measurements was in the range of 0.4–1 scan line/s.

For the STM measurements a chemically etched tungsten wire was used as a probe. The tunneling current was in a range of 1 nA with the sample bias of 1 V.

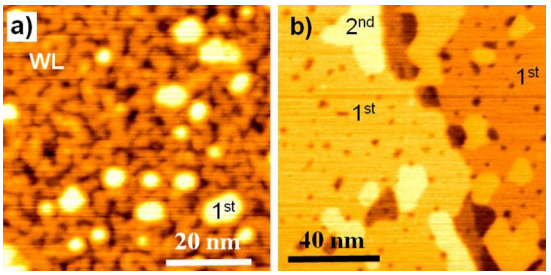


FIG. 2. (Color online) In (a) the STM topography of nominally 0.5 ML of Ag overlayer deposited on Ge(111) at 150 K and annealed to room temperature. The bright features correspond to the one monolayer high Ag islands supported on the intermixed layer of Ag and Ge, so-called wetting layer (WL). In (b) nc-AFM topography of nominally 1.5 ML of Ag overlayer deposited on Ge(111) at 150 K and annealed to room temperature.

## III. RESULTS AND DISCUSSION

### A. Evolution of the film morphology

Figure 2(a) is a typical STM topographic image of 0.5 ML of Ag, deposited on Ge(111) at 150 K, annealed to RT.

The background area, of a granularlike structure and the corrugation (rms) of about 0.6 Å, is the intermixed layer of Ag and Ge, so-called wetting layer (WL).[19] The big bright features are flat silver islands. The islands have only a single preferred height of about 2.5 Å as measured from the top of the wetting layer. The height of the bright island corresponds to one atomic layer of Ag. From the fractional coverage of the first layer islands we can estimate that about 0.3 ML of Ag is incorporated into the WL in agreement with the previous work.[21] Additional high-resolution STM measurements reveal the hexagonal shape of the island contour as would be expected for an island adopting the (111) termination.[12,19] Due to rather small Ag coverage and average island diameter around 5 nm, it is not possible to identify the Ag(111) signatures in the LEED pattern (data not shown). On the other hand, the LEED pattern indicates that Ag deposition at 150 K followed by annealing to room-temperature results in the disappearance of the Ge-$c(2\times 8)$ reconstruction, leaving only the Ge$(1\times 1)$ unreconstructed pattern.

In Fig. 2(b) we present the nc-AFM topography of the sample with an increased nominal Ag coverage of 1.5 ML. The layer corresponding to the flat bright islands in Fig. 2(a) appears now almost completely filled, leaving behind few pits of monoatomic depth. On top of the first layer, some extended monoatomic height islands are formed which are similarly bound by straight hexagonal steps. The height of the second layer islands measured from the first layer amounts to 2.14 Å, which corresponds closely to the Ag(111) interlayer spacing. The height of the compact first layer measured with respect to the substrate matches that of the islands in Fig. 2(a). In the image one can easily identify the presence of a step of the Ge substrate which is propagated vertically by the Ag film. The hexagonal symmetry of Ag layers is independently verified in the corresponding LEED pattern (data not shown) thus confirming that the Ag film is adopting a (111) epitaxy already from the first layer. By comparing the surface density of islands on top of the first Ag layer [Fig. 2(b)] which is lower by a factor of nine compare with that on top of the WL [Fig. 2(a)], we can conclude that the mobility of Ag adatoms on top of the first layer is significantly increased, as expected for Ag self-diffusion on Ag(111) ($E_d$=0.064–0.1 eV).[22] Based on the film morphology represented in Fig. 2(b), one might expect that the Ag film growth in the multilayer regime proceeds in a layer-by-layer growth mode.

Against these conclusions, stand the observations of the surface morphology after deposition of a higher amount of Ag, nominal coverage of 3 ML, as shown in Fig. 3. We follow the same procedure, i.e., deposition at 150 K followed by room-temperature annealing. In Fig. 3(a) we show the LEED pattern right after the deposition, before the room-temperature annealing. The only visible diffraction spots are those corresponding to the Ag(111) $(1\times 1)$ surface structure, with no spots characteristic of the Ge substrate, indicating that within the LEED sensitivity the deposit is forming a continuous film. After annealing [Fig. 3(b)] the LEED pattern changes markedly indicating presence of both the Ag(111) surface and the Ge(111) substrate surface. This is a clear indication that the film has undergone a morphological rearrangement, uncovering significant parts of the substrate.

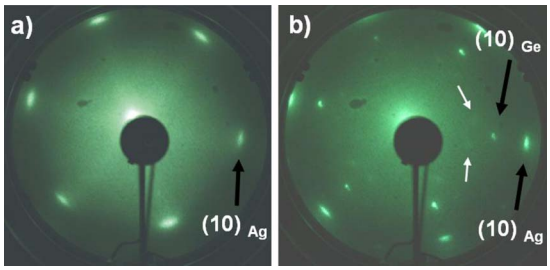


FIG. 3. (Color online) 3 ML Ag/Ge(111) LEED patterns taken right (a) after the LT (150 K) deposition and (b) after annealing to RT. In (b) the white arrows indicate the additional spots around the (1,0) spots which are assigned to a $(2\sqrt{3}\times 2\sqrt{3})R30°$ reconstruction.

From the LEED pattern we can also infer that the Ag(111) overlayer is formed epitaxially and incommensurate to the Ge(111) substrate. The significant lattice mismatch between Ag ($d_{\mathrm{Ag}}$=2.88 Å) and Ge ($d_{\mathrm{Ge}}$=4.00 Å) (Ref. 23) is compensated by the reconstruction of the wetting layer. The presence of a reconstructed WL is confirmed by the LEED pattern in Fig. 3(b) where faint additional spots commensurate to the Ge lattice can be observed around the (1,0) spots and assigned to a $(2\sqrt{3}\times 2\sqrt{3})R30°$ reconstruction.[19]

Direct evidence for the occurrence of a massive morphological reorganization of the Ag film is provided by the nc-AFM measurements shown in Fig. 4. The Ag continuous film converts into a network of "nanomesa" of 6 ML height with atomically flat tops and extended pits exposing the underlying wetting layer. In this case, it is hardly possible to find any Ag island which is topologically disconnected from the Ag network, i.e., which rests isolated on the WL in the middle of a pit. These observations are at variance with those made for Ag/Ag(111) self-epitaxy[24] where wedding-cake like mounds exposing several layers are found to be connected only through the lower supporting layer. The atomic steps bounding the edges are developing into considerably elongated ridges, reaching up to 100 nm, and appear to be predominantly oriented along the threefold symmetry of the (111) substrate. Due to the in equivalence of the thermodynamically favored step terminations on fcc(111) surfaces,[25] these can be attributed both to *A*-type steps, exposing (001) microfacets, and to *B*-type steps, exposing (111) microfacets.

These combined experimental findings indicate that during the RT annealing a massive fraction of Ag atoms residing

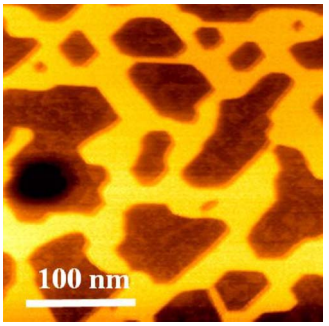


FIG. 4. (Color online) Nc-AFM topography of the nanomesa network created on Ge(111) substrate surface after deposition of 3 ML of Ag at LT (150 K) followed by annealing to RT.

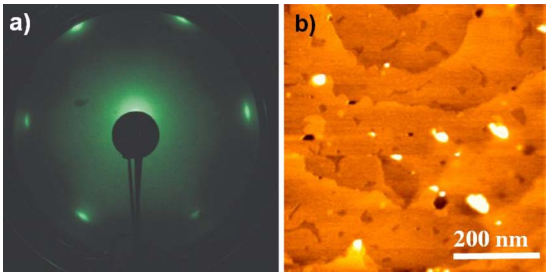


FIG. 5. (Color online) (a) LEED pattern and (b) nc-AFM topography of 6 ML Ag/Ge(111) overlayer after LT (150 K) deposition and annealing to RT.

initially in the low layers undergo true uphill diffusion to form six layer high nanomesas. Such a behavior could be driven by a thermodynamic minimization of the surface free energy in Stranski-Krastanov (SK) growth, but likely is also attributed to the presence of the energy minima at selected film heights due to quantum electron confinement (QSE).

In order to directly verify wherever the preferential population of the 6 ML thickness corresponds to an energy minimum of the Ag system and further investigate the stabilizing role of QSE, we have performed an experiment in which 6 ML of silver have been grown under the same experimental conditions as before (deposition at 150 K followed by room-temperature annealing). The LEED pattern [Fig. 5(a)] recorded at the end of the room-temperature annealing cycle shows the exclusive presence of reflections characteristic of the unreconstructed Ag(111) overlayer, a clear indication that the Ge substrate is completely buried. The morphology of the Ag overlayer is shown in the nc-AFM topography presented as Fig. 5(b). The film appears compact and uniform. Large, atomically flat terraces have sizes up to 0.2 $\mu$m across. The step structure of the underlying Ge substrate is propagated through the Ag overlayer, as evidenced by the steps height of 2.5 Å corresponding to the Ge step. A few small pits reaching down to the wetting layer can be found and used to determine the thickness of the Ag film with respect to the WL. In agreement with the Ag coverage determined using QSM, the top terrace corresponds to the sixth layer. There are also monoatomic pits [in this case the depth $h$=2.14 Å corresponds to the Ag(111) atomic step thickness] seen. The few bright spots which can be observed (average separation around 200 nm) are originated in correspondence to the pinning centers of the Ge steps, which survived the cleaning procedure of the pristine Ge substrate. The local structure of the Ag overlayer in their vicinity appears not to be affected in comparison to the areas in the middle of the extended terraces.

From the data just shown, we can infer that after low-temperature deposition the silver overlayer will statistically populate layers above the sixth, leaving behind equivalent unexposed areas in the layers below the sixth.[24] Upon annealing this additional material relaxes diffusing downward to fill the vacancies in the incomplete layers below the sixth, i.e., in this case a predominant net *downhill* mass transport is taking place. This experiment thus confirms that the formation of a compact 6-ML-thick overlayer corresponds to thermodynamic minimum state. The origin of the preferential

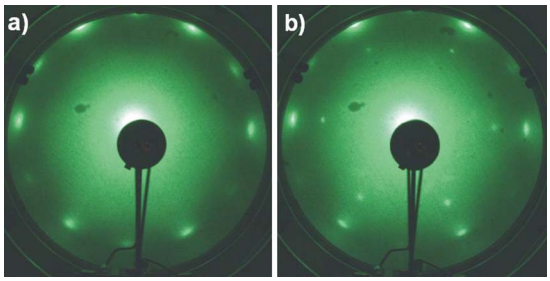


FIG. 6. (Color online) LEED patterns of sample surface after additional deposition of 3 ML of Ag on the overlayer formed by previous deposition of 3ML, like the one shown in Fig. 4, taken right (a) after the LT (150 K) deposition and (b) after annealing to RT.

occupation of 6 ML high islands can be thus attributed to the occurrence of quantum electronic stabilization (QSE). The occurrence of such layers of the preferred quantized heights is in agreement with the theoretical predictions based on the total-energy calculations described in Ref. 4. The observations are also in qualitative agreement with the closely related systems like of Ag/Si(111) (Ref. 8) and Ag/GaAs(110).[1]

The question arises if further energy minima can be accessed when the columnar mesa grows in height. In the first case, after the addition of further Ag on top of an incomplete sixth layer, like the one shown in Fig. 4, there should be a driving force biasing mass transport to maximize the occupancy of the sixth layer. We have thus performed an experiment in which three additional monolayers of Ag have been added to the system previously formed by deposition of 3 ML, like the one shown in Fig. 4.

Just after deposition at low temperature, the LEED pattern [Fig. 6(a)] reveals that the bottom of the pits exposing the WL has been completely filled by the additional Ag deposit (no Ge spots are observable). The Ag(111) spots originating from the top of the nanomesa are now accompanied by additional weak Ag(111) spots rotated by 30°, originating from the newly deposited film supported onto the WL at the bottom of the pits. The observed rotation of the Ag layer supported on the WL is connected to the reconstruction of the latter, which is rotated by 30° with respect to the Ge substrate over which the tall Ag structures are supported.

Upon annealing to room temperature the LEED pattern shows the disappearance of the additional Ag(111) weak spots [Fig. 6(b)] and at the same time shows the appearance of the Ge(111) reflexes, similar to the observations of Fig. 3(b). We can again indirectly conclude that upon RT annealing, the Ag film tends to decompose exposing extended portions of the underlying substrate.

Real space imaging of the overlayer morphology was accomplished by nc-AFM (Fig. 7). It is seen that the Ag film is transformed into a nanomesa network, with large atomically flat top layer and large flat portions of the WL. The predominant thickness is corresponding now to ten Ag(111) monolayers, with a small amount of the Ag stacked up to the 12th layer. Since the amount of additional material deposited on top of the film shown in Fig. 4 was enough to fill the preexisting pits and to produce a compact 6 ML thick overlayer, like that shown in Fig. 5(b), we can conclude that a signifi-

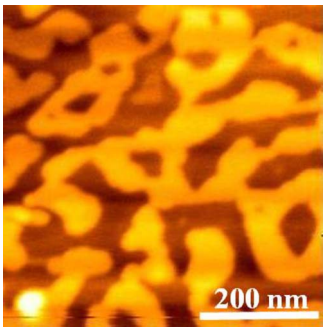


FIG. 7. (Color online) Nc-AFM topography of the nanomesa network created on Ge(111) substrate surface after additional deposition of 3 ML on top of the overlayer formed by deposition of 3 ML. The image was taken after annealing of the system to RT.

cant uphill mass transport of atoms from the pits to the top layers, across the nanomesa ridges has taken place during the annealing to room temperature. We can also imply that the energy of the 10-layer-thick Ag stack, corresponds to a minimum which appears to be lower than that of the 6-layer-thick configuration.

In Fig. 8 we sum up the observations concerning the occupancy of different layers after the film has relaxed at room temperature for all experiments performed in order to put these observations in a more quantitative form. An important issue to be considered deals with the kinetic pathways followed by the system in order to interrogate the minimum energy configurations located at higher elevations. The concerted diffusion of atoms residing in lower layers to form 6 or 10 ML high columns appears extremely unlikely, so other kinetic pathways accessible due to the initial low-

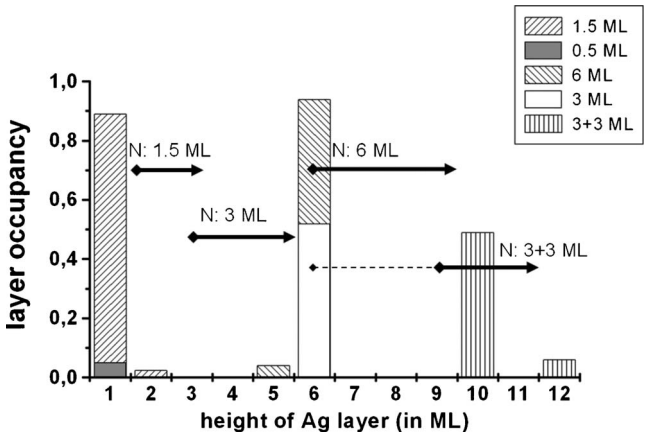


FIG. 8. Histogram of the fractional layer occupancy for the experiments corresponding to nominal deposition of 0.5, 1.5, 3, 6, and (3+3) ML of Ag on Ge(111) at 150 K followed by annealing to RT. The black arrows start from the nominal film thickness (diamond) and extend until the maximum overlayer thickness attainable within the Poisson growth model (the length correspond to the rms roughness of the deposited film for a sinusoidal height profile). In the case of (3+3) ML the second deposition step takes place on top of the incomplete 6 ML height supporting mesas. Thus, the arrow (straight line) reflecting the roughness of the film created during the second deposition step starts at (6+3) ML.

temperature morphology must be active. Indeed, under the chosen growth conditions at 150 K, due to the presence of the Ehrlich-Schwoebel barriers preventing downward atom diffusion at step edges, interlayer mass transport can be considered essentially negligible. The occupancy of the various layers after deposition can be well approximated by a Poisson growth model, in which the rms roughness of the deposited film W is simply related to the deposited coverage $\theta$, by the simple relation $W=\theta^{1/2}$, where both $W$ and $\theta$ are expressed in ML units.[26,27] In Fig. 8 the arrows represent the calculated interface width, equivalent to $\sqrt{2}$ rms, for the successive deposition experiments. In the case of deposition of 1.5 ML the probability of populating the sixth layer, thus reaching the local energy minimum is negligible, and the system relaxes into a flat configuration. In the case of deposition of 3 ML, according to the Poisson model the statistical population of levels up to 6 ML is statistically relevant. Thus, the system does relax to maximize the occupancy of this preferred thickness. On the other hand, after 6 ML deposition the occupancy of 6 ML high mesas is predominant already at low temperature even though the population of a smaller fraction at 10 ML height is possible. In this case, during relaxation at RT due to the predominant population of the sixth with respect to tenth layer, mass transport takes predominantly place downhill, thus filling the incomplete layers below the sixth one. The situation is instead different when additional three layers are deposited on top of the already relaxed 3 ML film, as shown in Fig. 4, which exposes a supporting top layer at 6 ML height. In this case levels up to the 12th layer can be statistically populated on top of the primitive supporting mesas, thus probing the energetically preferred tenth layer while the fractional population of sixth layer is completely reduced. Upon annealing to room temperature, the system now relaxes by maximizing the occupancy of the energetically favorable tenth layer; this implies the occurrence of a relevant uphill mass transport from the underlying layers which get depopulated until the WL is exposed.

The real-space imaging of the Ag/Ge(111), summarized in Fig. 8, demonstrates that low-temperature deposition of Ag followed by annealing to room temperature, leads to the growth of columnar islands with preferred height of 6, 10, and 12 ML, depending on the amount of material deposited in partial agreement with the observations of Basile *et al.*[12] However, we could not observe the occurrence of layer by layer growth with significant population of layers at intermediate coverage population. We believe that this discrepancy could be related to the different thermal history of the samples in the two experiments since, in order to allow the system to reach the observed metastable morphologies, a significant amount of mass transport from the non-favored heights to the preferred ones has to take place. Thus, if the annealing time is too short for the system to reach equilibrium, the final film morphology can be nonunivocally defined and layers at intermediate height can still be populated.

The phase separation of the Ag film into a mesalike morphology of quantized magic height 6, 10, and 12 ML provides a strong indication that electronic quantum confinement effects are determining the overall film energetics as was proposed for other closely related metal/semiconductor

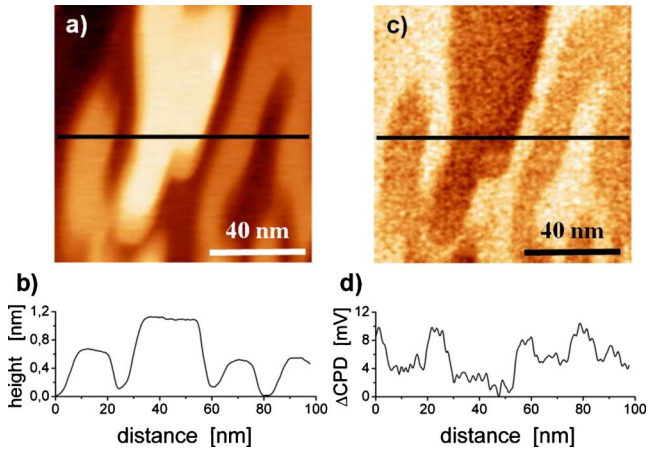


FIG. 9. (Color online) High-resolution KPFM imaging of Ag nanomesa network: topography map (a) with corresponding map of CPD signal (c). In (b) and (d) the height and CPD profiles taken along the lines on images (a) and (c), respectively, are shown.

growth pairs such as Ag/GaAs(110),[28] Pb/Si(111),[3] and Ag/Si(111).[5] The delicate interplay between energy minimization and growth kinetics is the deciding factor in determining the final film morphology. To form the mesalike Ag structures of preferred quantized height, a massive uphill mass transport has to take place from the bottom wetting layer toward the top of the mesas at 6, 10, and 12 ML height. The filling of the preferred layers at higher levels can take place only when the system is able to locally interrogate, those morphological configurations with minimum energy, thus providing the driving force for vertical mass transport.

### B. Surface potential measurements

The decomposition of the Ag overlayer into regions of selected thickness corresponding to energetically favored heights is known to affect several important properties such as the local surface potential.[2,13] A recent experimental verification was provided for the well studied Pb/Si(111) system,[29] where periodic oscillations of the work function amounting to 50 meV were observed in correspondence to a bilayer increases of the film thickness, i.e., in correspondence to the crossing of a QWS (quantum well state) below the Fermi edge.[30]

An ideal tool to probe the latter properties on a locally resolved lateral scale is Kelvin probe force microscopy which provides spatially resolved maps of surface potential and the corresponding topography with nanometer resolution.[31] In Fig. 9 the topography (a) of 3 ML Ag with the simultaneously acquired map of surface potential contrast (c) is shown. In the topography a part of the percolated nanomesa network formed by Ag layers of thickness of 2 and 4 ML appears to be supported on the WL. This is underlined in Fig. 9(b) where the height profile along the line in Fig. 9(a) shows that the lateral separation of the Ag nanomesas can be lower than 10 nm. Figure 9(c) represents the CPD signal acquired simultaneously with the topography. In the CPD map, the measured contact potential difference contrast closely matches with the corresponding topographic features,

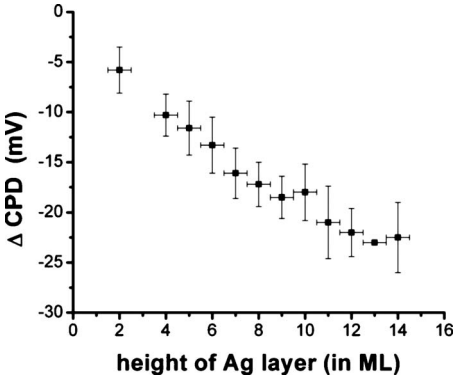


FIG. 10. Dependence of the CPD signal, as measured with respect to the WL, on the thickness of the Ag(111) nanomesas. The value of the work function difference saturates around −25 mV for Ag thicknesses exceeding 10 ML.

demonstrating the ability to laterally resolve the surface potential at nanometer scale. Such a lateral resolution of the CPD signal provides an example of the limits of the imaging with the KPFM technique operated in the frequency modulation mode.[32] The FM-KPFM technique is sensitive to the electrostatic force gradient, perpendicular to the sample surface, which decays faster the electrostatic tip-sample interaction itself. Thus, it implies that the tip apex is the most dominant part of the probe influencing the lateral resolution of the CPD signal. The sharp tip apex (so-called nanotip) increases the lateral resolution in the topography image but also in the CPD map as explained by recent calculations.[33] Such a sharp nanotip can be formed on the tip apex by picking up some material from surface in the process of uncontrolled tip-sample contact which often takes place during scanning the sample.[34]

The map shown in Fig. 9(c) represents the voltage applied to the sample in order to compensate the CPD between the surface and the tip therefore the dark contrast on the Ag film indicates that the surface potential (the work function) of the Ag overlayers is lower with respect to the work function of the WL. This observation is in agreement with the fact that the work function of the Ag(111) surface ($\Phi$=4.53 eV) (Ref. 35) is lower than that of the Ge(111) surface ($\Phi$=4.80 eV).[36] However, it should be stressed that the contact potential difference is not measured with respect to the pure Ge(111) surface but with respect to the WL layer which provides a lower contrast in the CPD signal. This is due to the incorporation of the Ag atoms into the reconstructed Ge(111) surface lattice, leading to a reduction in the bare Ge surface potential.[37] In Fig. 9(d) the cross-section profile taken along the line in Fig. 9(c) shows that the variation in the CPD signal originated on different height layers is of the order of 4 mV and varies on a lateral scale as small as 5 nm. We performed FM-KPFM in correspondence to all experimental cycles described so far, measuring the work function difference between different height levels, all referenced to the bottom layer (WL). The summary of these analyses is plotted in Fig. 10 where one can see a monotonic decrease in the CPD (with respect to the WL) when the thickness of the Ag(111) nanomesas increases. Though the statistical occupancy of the layers is dominated by the preferential heights,

as shown in Fig. 8, it is possible to find a very small fraction of the surface where the kinetic relaxation process is still taking place, leading to the statistically irrelevant population of layers of intermediate height. The value of the work function difference finally saturates around −25 mV for Ag thicknesses exceeding 10 ML. The lack of any oscillatory dependence of the CPD contrast in accordance with the film thickness, in particular in correspondence to preferential occupation of the layers with 6 and 10 ML height where the quantum size effect manifests itself, is at variance to the case of Ag(100) on Fe(100) (Ref. 2) where an oscillatory CPD variation in the range of 50 mV was observed recurring to spatially averaged photoemission experiments. In the latter case the density of states at the Fermi level undergoes an abrupt jump every time a new QWS crosses the Fermi level thus inducing a modulation of the work function. Also in the case of Pb/Si(111) (Ref. 38) similar work function oscillations with a bilayer periodicity have been attributed to the crossing of a QWS below the Fermi level; in correspondence the density of states at the Fermi level is higher and the spatial spill out of the electronic wave functions (responsible for the surface dipole formation) is there maximized.

In order to explain the observed dependence of CPD on the Ag nanomesa thickness, and due to a lack of accurate calculations of electronic structure of the thin Ag film, one can adopt the projected bulk band structure of an Ag(111) slab.[39] In the case of (111) termination of the Ag the electronic structure has a peculiar behavior since it presents a gap of about 0.3 eV in the [111] direction (perpendicular to the surface);[40] this means that no electron propagation is allowed along [111] for electrons with energy between the Fermi level and the top of the valence band. In this case one can expect a modulation of the electron density of states only when the QWS crosses the top of the valence band located 0.3 eV below the Fermi level. For these deeper lying electron states the spatial spill out of the wave functions is reduced which in turn leads to a weaker oscillation of the work function with film thickness. The present experimental observations lead us to conclude that, within the experimental resolution of about 5 mV, the effect is not observable.

## IV. SUMMARY

In summary, we have investigated the morphological evolution of low-temperature deposited Ag ultrathin films (0.5–6 ML) supported on Ge(111)-$c(2\times8)$ by means of SPM real-space imaging. The experiments demonstrate that, after annealing to room temperature, the metal film reorganizes into a network of metastable nanomesas of quantized heights, which adopt a perfect (111) epitaxy on top of the supporting wetting layer. This implies that, in order to allow the relaxation of the film morphology, massive uphill mass transport has to take place. The metastable morphology of the Ag film is determined by a delicate interplay between thermodynamics and the kinetics of interlayer mass transport. The preferential population of a discrete set of metastable heights at 6, 10, and 12 ML suggests that quantum size effects are active and drive the morphological evolution of the film in similar fashion to the closely related Ag/Si(111) case.

The laterally resolved maps of the contact potential difference of the system were acquired by means of Kelvin probe force microscopy, providing clear evidence of a monotonic, layer-dependent CPD contrast with lateral resolution of few nm, and energy resolution in the range of few meV. This has been found to be at variance with the observations made on Ag(001) films where an oscillatory behavior was observed in correspondence to the height changes. The discrepancy has probably to do with the difference in the electronic band structure of Ag(111) which presents a gap in the direction perpendicular to the surface.

## ACKNOWLEDGMENTS

This work was supported by the Italian Ministry of Foreign Affairs (MAE) under program "Italia-Polonia," by MIUR under project PRIN 2008J858Y7 and by the Seventh Framework Programme of the European Commission within the Coordination Action "Nano-scale ICT Devices and Systems, NanoICT" (Contract No. 216165). One of us (M.S.) would like to acknowledge the support received from the Polish Foundation for Science (Contract for Subsidy No. 11/2007).

*FAX: +48 12 6337086; franciszek.krok@uj.edu.pl

[1] A. R. Smith, K.-J. Chao, Q. Niu, and C.-K. Shih, Science **273**, 226 (1996).
[2] J. J. Paggel, C. M. Wei, M. Y. Chou, D.-A. Luh, T. Miller, and T.-C. Chiang, Phys. Rev. B **66**, 233403 (2002).
[3] A. Menzel, M. Kammler, E. H. Conrad, V. Yeh, M. Hupalo, and M. C. Tringides, Phys. Rev. B **67**, 165314 (2003).
[4] Z. Zhang, Q. Niu, and C.-K. Shih, Phys. Rev. Lett. **80**, 5381 (1998).
[5] L. Gavioli, K. R. Kimberlin, M. C. Tringides, J. F. Wendelken, and Z. Zhang, Phys. Rev. Lett. **82**, 129 (1999).
[6] L. Huang, S. J. Chey, and J. H. Weaver, Surf. Sci. **416**, L1101 (1998).
[7] S.-J. Tang, T. Miller, and T.-C. Chiang, Phys. Rev. Lett. **96**, 036802 (2006).
[8] S.-J. Tang, W.-K. Chang, Y.-M. Chiu, H.-Y. Chen, C.-M. Cheng, K.-D. Tsuei, T. Miller, and T.-C. Chiang, Phys. Rev. B **78**, 245407 (2008).
[9] Y. Liu, N. J. Speer, S.-J. Tang, T. Miller, and T.-C. Chiang, Phys. Rev. B **78**, 035443 (2008).
[10] S.-J. Tang, L. Basile, T. Miller, and T.-C. Chiang, Phys. Rev. Lett. **93**, 216804 (2004).
[11] K. Sawa, Y. Aoki, and H. Hirayama, Phys. Rev. B **80**, 035428 (2009).
[12] L. Basile, H. Hong, P. Czoschke, and T. C. Ciang, Appl. Phys. Lett. **84**, 4995 (2004).
[13] P. J. Feibelman and D. R. Hamann, Phys. Rev. B **29**, 6463 (1984).

[14] M. Nonnenmacher, M. P. O'Boyle, and H. K. Wickramasinghe, Appl. Phys. Lett. **58**, 2921 (1991).
[15] J. M. R. Weaver and D. W. Abraham, J. Vac. Sci. Technol. B **9**, 1559 (1991).
[16] S. Kitamura and M. Iwatsuki, Appl. Phys. Lett. **72**, 3154 (1998).
[17] Ch. Sommerhalter, Th. W. Matthes, Th. Glatzel, and A. Jaeger-Waldau, Appl. Phys. Lett. **75**, 286 (1999).
[18] D. J. Chadi and C. Chiang, Phys. Rev. B **23**, 1843 (1981).
[19] M. Padovani, E. Magnano, G. Bertoni, V. Spreafico, L. Gavioli, and M. Sancrotti, Appl. Surf. Sci. **212-213**, 213 (2003).
[20] F. Krok, J. J. Kolodziej, B. Such, P. Czuba, P. Struski, P. Piatkowski, and M. Szymonski, Surf. Sci. **566-568**, 63 (2004).
[21] H. M. Zhang and R. I. G. Uhrberg, Surf. Sci. Lett. **546**, L789 (2003).
[22] P. Stoltze, J. Phys.: Condens. Matter **6**, 9495 (1994).
[23] R. R. Lieten, S. Degroote, K. Cheng, M. Leys, M. Kuijk, and G. Borghs, Appl. Phys. Lett. **89**, 252118 (2006).
[24] P.-W. Maozhi Li, Chung, E. Cox, C. J. Jenks, P. A. Thiel, and J. W. Evans, Phys. Rev. B **77**, 033402 (2008).
[25] H. Brune, H. Roder, C. Boragno, and K. Kern, Phys. Rev. Lett. **73**, 1955 (1994).
[26] E. Z. Luo, J. Wollschläger, F. Wegner, and M. Henzler, Appl. Phys. A: Mater. Sci. Process. **60**, 19 (1995).
[27] J. W. Evans, P. A. Thiel, and M. C. Bartelt, Surf. Sci. Rep. **61**, 1 (2006).
[28] H. Yu C. S. Jiang, Ph. Ebert, X. D. Wang, J. M. White, Q. Niu, Z. Zhang, and C. K. Shih, Phys. Rev. Lett. **88**, 016102 (2001).
[29] P. S. Kirchmann, M. Wolf, J. H. Dil, K. Horn, and U. Bovensiepen, Phys. Rev. B **76**, 075406 (2007).
[30] H. Okamoto, D. Chen, and T. Yamada, Phys. Rev. Lett. **89**, 256101 (2002).
[31] U. Zerweck, Ch. Loppacher, T. Otto, S. Grafstrom, and L. M. Eng, Phys. Rev. B **71**, 125424 (2005).
[32] F. Krok, K. Sajewicz, J. Konior, M. Goryl, P. Piatkowski, and M. Szymonski, Phys. Rev. B **77**, 235427 (2008).
[33] F. Bocquet, L. Nony, C. Loppacher, and T. Glatzel, Phys. Rev. B **78**, 035410 (2008).
[34] C. Barth and C. R. Henry, J. Phys. Chem. C **113**, 247 (2009).
[35] H. B. Michaelson, J. Appl. Phys. **48**, 4729 (1977).
[36] G. W. Gobeli and F. G. Allen, Phys. Rev. **137**, A245 (1965).
[37] H. Y. Xiao and X. T. Zu, Physica B **371**, 50 (2006).
[38] Y.-F. Zhang, J.-F. Jia, T.-Z. Han, Z. Tang, Q.-T. Shen, Y. Guo, Z. Q. Qiu, and Q.-K. Xue, Phys. Rev. Lett. **95**, 096802 (2005).
[39] S.-J. Tang, Y.-R. Lee, S.-L. Chang, T. Miller, and T.-C. Chiang, Phys. Rev. Lett. **96**, 216803 (2006).
[40] T.-C. Chiang, Surf. Sci. Rep. **39**, 181 (2000).